Supporting Information for

"Drastic Tuning of the Electronic Structures of Diruthenium Aryl Complexes by Isoelectronic Axial Ligands"

*Adharsh Raghavan, Fang Yuan and Tong Ren**

TABLE OF CONTENTS

1. Experimental details …… S3
2. Mass spectrometry (ESI-MS)
   - **Figure S1**. ESI-MS of (NC)Ru_2(*ap*)$_4$(C_6H_4-4-NMe_2) (**2**)…… S5
   - **Figure S2**. ESI-MS of (HCC)Ru_2(*ap*)$_4$(C_6H_4-4-NMe_2) (**3**) ……..…..… S6
   - **Figure S3**. ESI-MS of (OC)Ru_2(*ap*)$_4$(C_6H_4-4-NMe_2) (**4**) ……... S7
3. Crystallographic details
   - **Table S1**. Selected bond metrics for **2**–**4** …… S9
   - **Table S2**. Crystallographic details for **2** ……. S10
   - **Table S3**. Crystallographic details for **3** ……. S11
   - **Table S4**. Crystallographic details for **4** ……. S12
4. ^{1}H NMR spectroscopy
   - **Figure S4**. ^{1}H NMR spectrum of **2** at 293 K in $CDCl_3$ …..…….. S12
   - **Figure S5**. ^{1}H NMR spectrum of **3** at 293 K in $CDCl_3$ ..……..….. S13
   - **Figure S6**. Evans method magnetometry of **4** in C_6D_6 ……. S14
   - **Figure S7a-b**. Variable temperature (VT) NMR spectrum of **3** in $CDCl_3$ ……... S15
   - **Figure S8a-c**. VT-NMR chemical shift analyses for C≡C–**H**, N(C**H**$_3$)$_2$ and aryl(C**H**) protons of **3** …… S16–17
5. Electrochemistry
   - **Figure S9**. Cyclic and Differential Pulse Voltammetry of **2**–**4** ……. S18
   - **Table S5**. Redox potentials for **1**–**4** ……... S18
   - **Table S6**. Voltammetry and IR spectroscopy of Ru_2–CO complexes in the literature ……... S19
6. Dissociation of CO from compound **4**
   - **Figure S10**. UV-Vis/NIR absorption spectrum …..……... S20
   - **Figure S11**. Cyclic Voltammogram of **1** and **4** …..……... S20
7. SQUID magnetometry
   - **Figure S12**. χ_m and μ_{eff} vs. T, **1** ……. S21
   - **Figure S13**. χ_m and μ_{eff} vs. T, **4** ……. S22
8. Computational details
   - **Figure S14**. DFT optimized structure of **4** ….……..……. S23
   - **Table S7**. Bond metrics of the optimized structure **4′** …….. S23
   - **Figure S15**. Frontier molecular orbitals of **4′** …… S24
   - **Figure S16**. Mulliken spin density plot for **4′** …….……... S24
   - **Figure S17**. TD-DFT-calculated spectrum of **4′** ……. S25
9. References ……...…….. S25–S26

EXPERIMENTAL DETAILS

General. $Ru_2(ap)_4Cl$[1] and $Ru_2(ap)_4(C_6H_4\text{-}4\text{-}NMe_2)$ (**1**)[2] were prepared using literature methods. ^{n}BuLi (1.6 M in hexanes) was purchased from Sigma-Aldrich. Bis(trimethylsilyl)-1,3-butadiyne was purchased from Alfa Aesar and freshly sublimed before use. Sodium acetylide (18 wt% slurry in xylene, ρ = 0.89 g/mL) was purchased from Sigma-Aldrich. KCN and $[^nBu_4N][PF_6]$ were purchased from commercial sources and used as received. Tetrahydrofuran was freshly distilled over sodium/benzophenone prior to use. All reactions were performed under dry N_2 atmosphere implementing standard Schlenk techniques where noted. UV-Vis/NIR spectra were obtained with a JASCO V-670 spectrophotometer in THF solutions. ^{1}H NMR spectra were recorded on a Varian Inova 300 spectrometer operating at 300 MHz. Cyclic and differential pulse voltammograms were recorded in 0.1 M $[^nBu_4N][PF_6]$ solution (THF, Ar or N_2-degassed) on a CHI620A voltammetric analyzer with a glassy carbon working electrode (diameter = 2 mm), a Pt-wire auxiliary electrode, and a Ag/AgCl quasi-reference electrode. The concentration of Ru_2-species is always ca. 1.0 mM. The $Fc^{+/0}$ couple was observed at ca. 0.542 ± 0.113 V (vs Ag/AgCl QRE) at the noted experimental conditions. Electrospray ionization mass spectra (ESI-MS) were collected on an Advion express**ion**^{L} mass spectrometer with an m/z range of 10 – 2000. Elemental analyses were performed by Atlantic Microlab, Inc. DC temperature-dependent magnetization was measured from 2 to 300 K using zero-field-cooling (ZFC) mode on a Quantum Design MPMS-3 SQUID magnetometer. Both compound **1** and **4** were measured under a magnetic field of 1000 Oe with a cooling rate of 2 K/min. The whole magnetic measurement was done under vacuum of a few torr.

Synthesis of (N≡C)Ru_2(*ap*)$_4$(C_6H_4-4-NMe_2) (2). To a 20 mL solution of **1** (60 mg, 0.06 mmol) in THF was added a 10 mL solution of KCN 20 mg, 0.31 mmol) in MeOH. A rapid color change from black to deep red/purple was observed. O_2 was bubbled through the reaction mixture for 10 minutes during which a distinct color to violet was observed. The solvents were removed in vacuo and the product was extracted from CH_2Cl_2/H_2O. The organic layers were collected, and the product was recrystallized from a 1:20 (v:v) CH_2Cl_2:hexanes mixture at −20°C, as a dark violet microcrystalline solid. Yield: 51 mg, 83%. Crystals suitable for X-ray diffraction analysis were grown by layering hexanes over a concentrated solution of **2** in THF.

Data for **2**. Anal. Found (Calcd.) for $C_{54}H_{50}N_{10}OCl_2Ru_2$ (**2**·CH_2Cl_2·H_2O): C, 57.52 (57.49); H, 4.43 (4.47); N, 12.34 (12.42). ESI-MS (m/z, based on ^{101}Ru): $[M+H]^+$ = 1027.4. UV-Vis (in THF) λ, nm, (ε, $M^{-1}cm^{-1}$): 345 (13000), 440 (2500, sh), 550 (4000), 600 (3900), 667 (3500), 740 (2400, sh), 1014 (2900). IR $\bar{\nu}$, cm^{-1}: 2084, ν(C≡N). Electrochemistry (THF, vs. $Fc^{+/0}$), $E_{1/2}$/V, ΔE_p/mV, $i_{forward}/i_{backward}$: −0.11, 64, 1.1; 0.30, 62, 1.2; −0.98, 65, 1.1. ^{1}H NMR (300 MHz, 293 K, $CDCl_3$) δ = 3.21 (s, 6H, N(C*H*$_3$)$_2$), 5.60 (br, 4H, *ap*), 6.07 (t, 8H, *ap*, 6.4 Hz), 6.14 (d, 2H, aryl, 6.6 Hz), 6.28 (d, 4H, *ap*, 9.0 Hz), 6.69 (d, 2H, aryl, 6.6 Hz), 6.77–7.21 (m, 16H, *ap*), 7.99 (d, 4H, *ap*, 6.9 Hz).

Synthesis of (HC≡C)Ru$_2$(*ap*)$_4$(C$_6$H$_4$-4-NMe$_2$) (3). Sodium acetylide slurry (1.1 mL, 18 wt%, ca. 3.7 mmol) was added to a 10 mL THF solution of **1** (60 mg, 0.060 mmol). The color of the solution gradually changed from red-black to blue-black over the course of 24 h under N_2. Aliquots of the reaction mixture were retrieved for TLC analysis. The ratio of the starting material to product (ca. 2:3) did not noticeably change after 24–36 h despite addition of excess sodium acetylide. At this juncture, O_2 was bubbled through the reaction mixture for 30 minutes. The crude reaction mixture was purified by column chromatography. The blue fraction was eluted with triethylamine/EtOAc/hexanes (1/10/70, v/v/v). Yield: 22 mg, 36%. Crystals suitable for X-ray diffraction analysis were grown by layering hexanes over a concentrated solution of **3** in THF.

Data for **3**. Anal. Found (Calcd.) for $C_{62}H_{71}N_9O_6Ru_2$ (**3**·2THF·4H_2O): C, 59.78 (60.03); H, 5.45 (5.77); N, 9.90 (10.16). ESI-MS (m/z, based on ^{101}Ru): [M^+] = 1024.2. UV-Vis (in THF) λ, nm, (ε, $M^{-1}cm^{-1}$): 345 (25000, sh), 450 (5600, sh), 570 (7000, sh), 641 (9700), 740 (5800, sh), 1060 (3600). IR $\bar{\nu}$, cm^{-1}: 1947, ν(C≡C); 3280, ν(C≡**C-H**). Electrochemistry (THF, vs. $Fc^{+/0}$), $E_{1/2}$/V, ΔE_p/mV, $i_{forward}/i_{backward}$: −0.21, 66, 1.1; 0.21, 67, 1.2; −1.2, 71, 1.2; −1.53, 188, 1.4. ^{1}H NMR (300 MHz, 293 K, $CDCl_3$) δ = −10.74 (s, 1H, C≡C*H*), 1.39 (d, 2H, aryl, 8.4 Hz), 2.99 (t, 4H, *ap*, 6.3 Hz), 3.90 (d, 4H, *ap*, 8.8 Hz), 5.34 (br, 4H, *ap*), 5.66 (s, 6H, N(CH_3)$_2$), 5.92 (br, 4H, *ap*), 6.86 (t, 4H, *ap*, 6.9 Hz), 6.96 (d, 2H, aryl, 8.4 Hz), 7.49 (br, 8H, *ap*), 8.00 (t, 4H, *ap*, 7.5 Hz), 3.90 (d, 4H, *ap*, 6.9 Hz).

Synthesis of (O≡C)Ru$_2$(*ap*)$_4$(C$_6$H$_4$-4-NMe$_2$) (4). Carbon monoxide gas was bubbled through a 20 mL THF solution of **1** (50 mg, mmol) in a Schlenk tube. An immediate colour change from red-black to deep red was observed. Solvent was evaporated and the red solid thus obtained was dried in vacuo. Prior to collecting the solid for analysis, the tube was re-pressurized with $CO_{(g)}$. Yield: 51 mg, 99 %. Crystals suitable for X-ray diffraction analysis were grown in a tube sealed with a slight pressure of $CO_{(g)}$ by layering hexanes over a concentrated solution of **4** in a 1:1 mixture of benzene and toluene.

Data for **4**. Anal. Found (Calcd.) for $C_{53}H_{52}N_9O_4Ru_2$ (**4**·3H_2O): C, 58.97 (58.88); H, 4.46 (4.85); N, 11.23 (11.66). Loss of the labile CO is possible during shipping and handling of the EA sample. ESI-MS (m/z, based on ^{101}Ru): [$M]^+$ = 1028.2, [M−CO]$^+$ = 1000.2. UV-Vis (in THF) λ, nm, (ε, $M^{-1}cm^{-1}$): 336 (33000, sh), 486 (6300), 815 (5700), 1010 (2800, sh). IR $\bar{\nu}$, cm^{-1}: 1950, ν(C≡O). μ_{eff} (25°C) = 1.9 B.M. Electrochemistry (THF, vs. $Fc^{+/0}$), $E_{1/2}$/V, ΔE_p/mV, $i_{forward}/i_{backward}$: −0.34, 63, 1.03; 0.18, 57, 1.04; −1.39, 59, 1.00.

Attempted reactions of CO with [Ru$_2$(ap)$_4$]X (X = Cl, CN, C≡CR, N$_3$): The Ru_2 starting materials were prepared via established literature procedures through metathesis reactions of $Ru_2(ap)_4Cl$ with KCN,[3] MC≡CR (M = Li, R = Ph, C$_6$H$_4$-4-NMe$_2$, M = Na, R = H)[4,5] and NaN_3,[6] respectively. CO was bubbled through THF solutions of [$Ru_2(ap)_4$]X for ca. 1 min at room temperature. When no color change was observed, the reaction was attempted at an elevated

temperate (50–60 °C) for ca. 1 min. No color change was observed, and ESI-MS of the reaction mixtures consistently showed no new product peaks.

MASS SPECTROMETRY (ESI-MS)

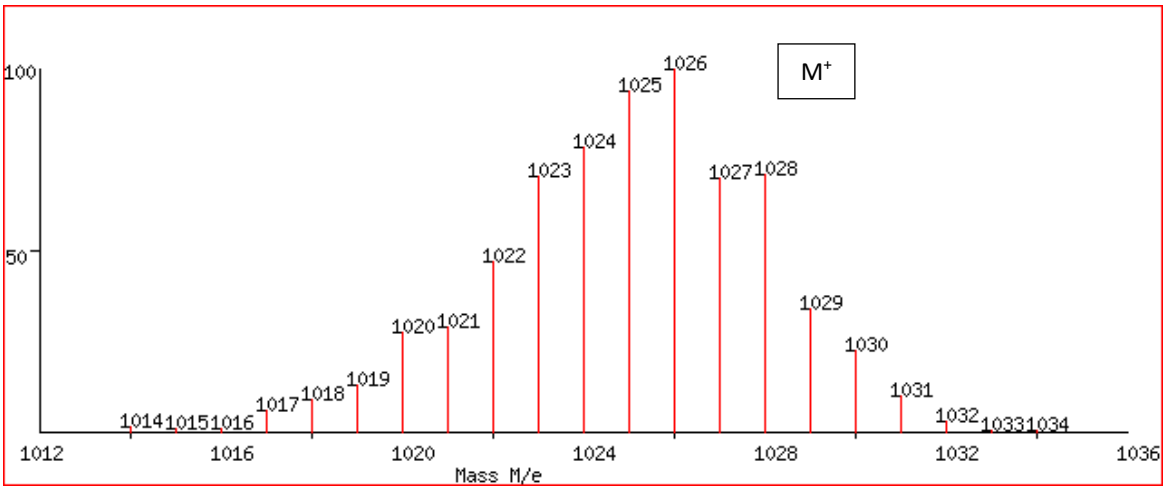

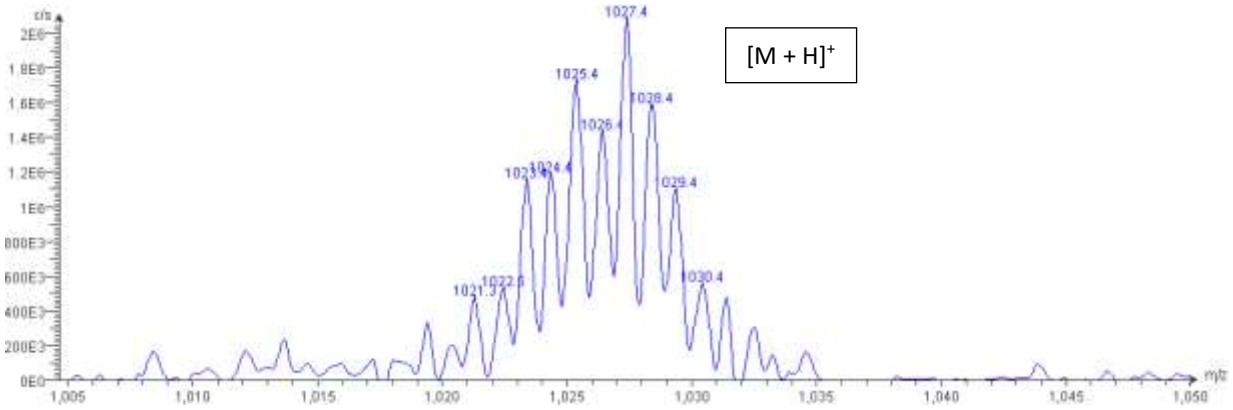

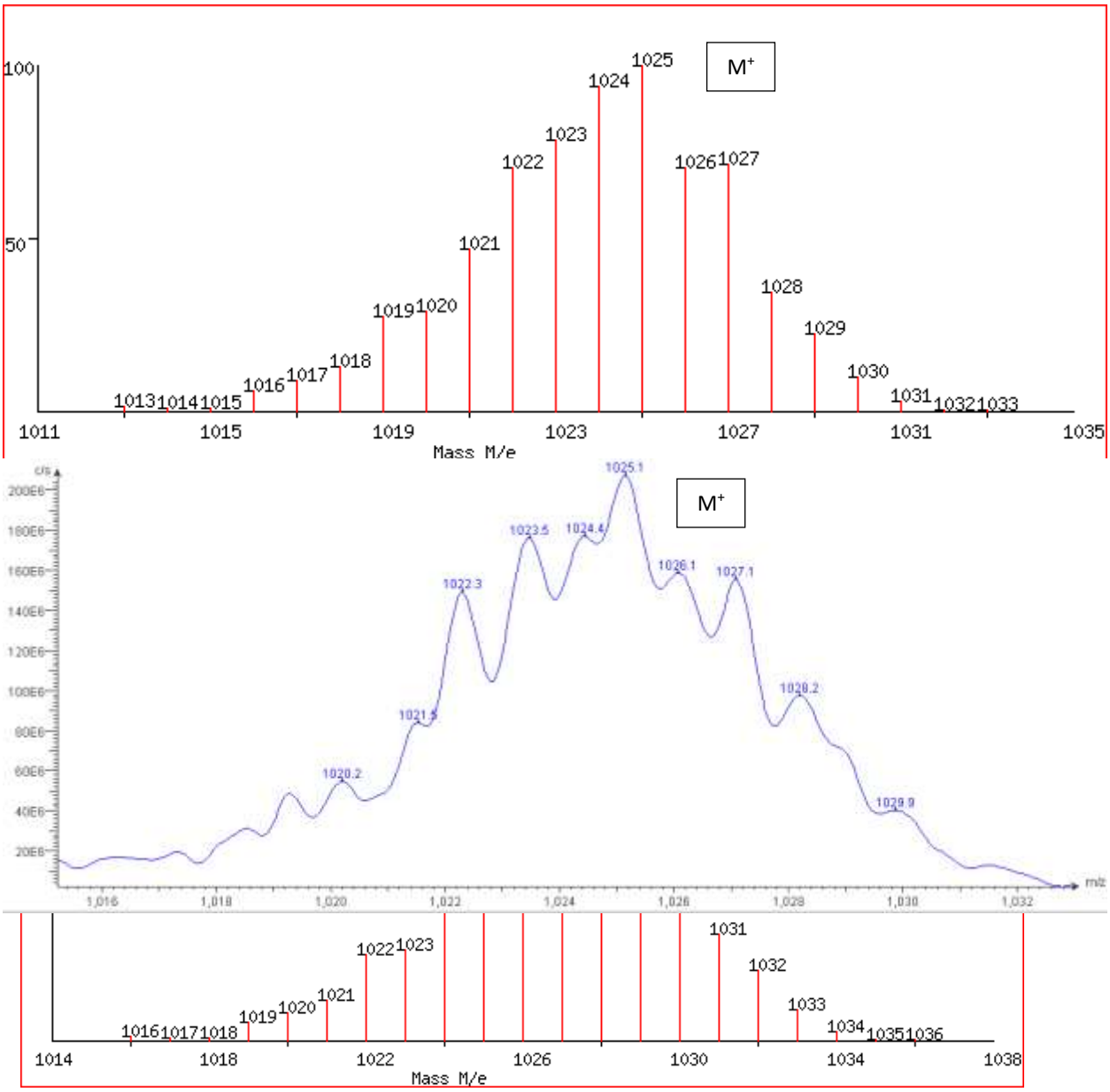
100
50
M+
1025
1024
1023
1022
1026
1027
1021
1028
1029
1019
1020
1030
1018
1031
1016
1017
1013
1014
1015
1032
1033
1011
1015
1019
1023
1027
1031
1035
Mass M/e

M+
1025.1
1023.5
1024.4
1022.3
1026.1
1027.1
1021.5
1028.2
1020.2
1029.9
m/z

1022
1023
1031
1032
1019
1020
1021
1033
1016
1017
1018
1034
1035
1036
1014
1018
1022
1026
1030
1034
1038
Mass M/e

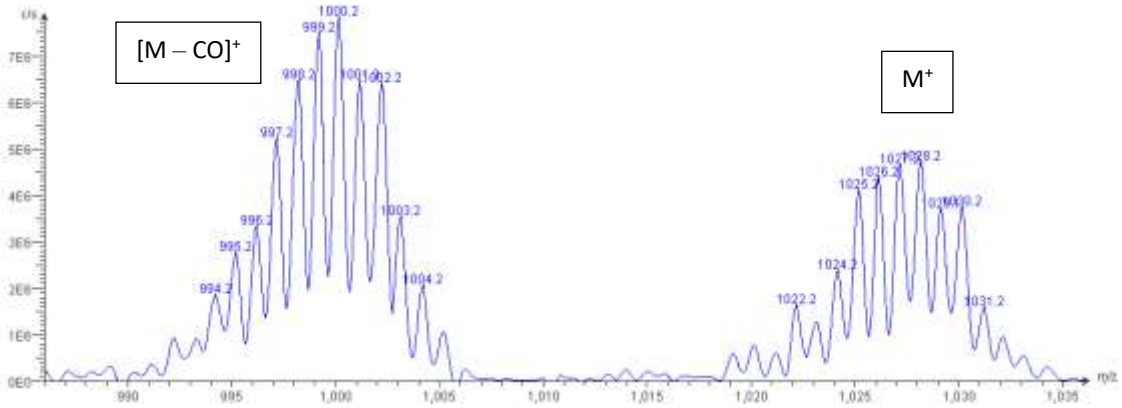
[M – CO]+
M+
m/z

CRYSTALLOGRAPHIC DETAILS

Single-crystal X-ray diffraction data for compounds **2**−**4** at 150 K were collected on a Bruker AXS D8 Quest CMOS diffractometer using Mo-Kα radiation (λ = 0.71073 Å). Data was collected and processed using APEX3, and the structures were solved using SHELXT suite of programs and refined to convergence on F^2 and against all independent reflections by full-matrix least-squares using SHELXL.[7-9] All non-hydrogen atoms were refined anisotropically and hydrogen atoms were geometrically placed and allowed to ride on their parent atoms.

CCDC 2000255-2000257 contain the supplementary crystallographic data for this paper. These data can be obtained free of charge via www.ccdc.cam.ac.uk/data_request/cif, or by emailing data_request@ccdc.cam.ac.uk, or by contacting The Cambridge Crystallographic Data Centre, 12 Union Road, Cambridge CB2 1EZ, UK; fax: +44 1223 336033.

Table S1. Selected Bond Lengths (Å) and Angles (deg) for Compounds **2**−**4**.

	2, CN	**3, CCH**	**4, CO**
Ru1−Ru2	2.4857(7)	2.4887(5)	2.5060(3)
Ru1−C1	2.077(7)	2.058(4)	2.053(2)
Ru2−C53	2.021(7)	2.005(4)	1.877(2)
C53−N10/C54/O1	1.14(1)	1.181(6)	1.146(2)
Ru2−Ru1−C1	157.0(2)	156.02(9)	155.61(6)
Ru1−Ru2−C53	166.9(2)	166.45(9)	169.50(7)
Ru1−N1	2.149(5)	2.132(2)	2.157(2)
Ru1−N3	2.138(5)	2.156(2)	2.040(1)
Ru1−N5	2.038(4)	2.038(2)	2.068(2)
Ru1−N7	2.037(5)	2.018(3)	2.166(1)
Ru2−N2	1.974(5)	2.007(2)	2.028(2)
Ru2−N4	1.988(5)	1.978(3)	2.136(2)
Ru2−N6	2.068(5)	2.080(2)	2.069(2)
Ru2−N8	2.165(4)	2.164(2)	2.022(1)

Table S2. Crystallographic details for $(NC)Ru_2(ap)_4(C_6H_4\text{-}4\text{-}NMe_2)$ (**2**)

	AR_3_21_0m (CCDC 2000255)
Crystal data	
Chemical formula	$C_{61}H_{62}N_{10}O_2Ru_2$
M_r	1169.34
Crystal system, space group	Monoclinic, $P2_1/c$
Temperature (K)	150
a, b, c (Å)	19.0728 (8), 16.6306 (7), 18.7099 (7)
β (°)	117.995 (2)
V (Å^3)	5240.2 (4)
Z	4
Radiation type	Cu $K\alpha$
μ (mm^{-1})	5.10
Crystal size (mm)	0.2 × 0.1 × 0.05
Data collection	
Diffractometer	Bruker AXS D8 Quest CMOS diffractometer
Absorption correction	Multi-scan *SADABS* 2016/2: Krause, L., Herbst-Irmer, R., Sheldrick G.M. & Stalke D. (2015). J. Appl. Cryst. 48 3-10.
T_{min}, T_{max}	0.477, 0.754
No. of measured, independent and observed [$I > 2\sigma(I)$] reflections	35321, 10759, 7585
R_{int}	0.091
$(\sin\theta/\lambda)_{max}$ (Å^{-1})	0.640
Refinement	
$R[F^2 > 2\sigma(F^2)]$, $wR(F^2)$, S	0.061, 0.174, 1.07
No. of reflections	10759
No. of parameters	678
H-atom treatment	H-atom parameters constrained
$\Delta\rangle_{max}$, $\Delta\rangle_{min}$ (e Å^{-3})	1.39, -1.37

Table S3. Crystallographic details for (HCC)$Ru_2(ap)_4(C_6H_4$-4-$NMe_2)$ (**3**)

	AR_3_173_0m (CCDC 2000256)
Crystal data	
Chemical formula	$C_{62}H_{63}N_9O_2Ru_2$
M_r	1168.35
Crystal system, space group	Triclinic, $P\bar{1}$
Temperature (K)	150
a, *b*, *c* (Å)	11.3227 (5), 14.1697 (6), 17.6704 (7)
α, β, γ (°)	109.063 (2), 102.115 (3), 92.949 (3)
V (Å^3)	2597.70 (19)
Z	2
Radiation type	Cu *K*α
μ (mm^{-1})	5.14
Crystal size (mm)	0.20 × 0.15 × 0.14
Data collection	
Diffractometer	Bruker AXS D8 Quest CMOS diffractometer
Absorption correction	Multi-scan *SADABS* 2016/2: Krause, L., Herbst-Irmer, R., Sheldrick G.M. & Stalke D. (2015). J. Appl. Cryst. 48 3-10.
T_{min}, T_{max}	0.530, 0.753
No. of measured, independent and observed [$I > 2\sigma(I)$] reflections	29336, 9759, 8521
R_{int}	0.057
$(\sin\theta/\lambda)_{max}$ (Å^{-1})	0.610
Refinement	
$R[F^2 > 2\sigma(F^2)]$, $wR(F^2)$, *S*	0.040, 0.114, 1.01
No. of reflections	9759
No. of parameters	724
No. of restraints	216
H-atom treatment	H-atom parameters constrained
$\Delta\rangle_{max}$, $\Delta\rangle_{min}$ (e Å^{-3})	1.24, -1.30

Table S4. Crystallographic details for $(OC)Ru_2(ap)_4(C_6H_4\text{-}4\text{-}NMe_2)$ (**4**)

	AR_3_99_0m (CCDC 2000257)
Crystal data	
Chemical formula	$C_{59.39}H_{52.77}N_9ORu_2$
M_r	1110.66
Crystal system, space group	Triclinic, $P\bar{1}$
Temperature (K)	150
a, *b*, *c* (Å)	12.5822 (9), 12.8242 (9), 17.5440 (11)
α, β, γ (°)	71.387 (3), 73.114 (2), 75.340 (3)
V (Å^3)	2526.7 (3)
Z	2
Radiation type	Mo *K*α
μ (mm^{-1})	0.65
Crystal size (mm)	0.70 × 0.30 × 0.30
Data collection	
Diffractometer	Bruker AXS D8 Quest CMOS diffractometer
Absorption correction	Multi-scan *SADABS* 2016/2: Krause, L., Herbst-Irmer, R., Sheldrick G.M. & Stalke D., J. Appl. Cryst. 48 (2015) 3-10
T_{min}, T_{max}	0.674, 0.746
No. of measured, independent and observed [$I > 2\sigma(I)$] reflections	83101, 16824, 13493
R_{int}	0.036
$(\sin\theta/\lambda)_{max}$ (Å^{-1})	0.737
Refinement	
$R[F^2 > 2\sigma(F^2)]$, $wR(F^2)$, S	0.034, 0.075, 1.08
No. of reflections	16824
No. of parameters	707
No. of restraints	204
H-atom treatment	H-atom parameters constrained
$\Delta\rangle_{max}$, $\Delta\rangle_{min}$ (e Å^{-3})	2.81, -1.13

^{1}H NMR SPECTROSCOPY

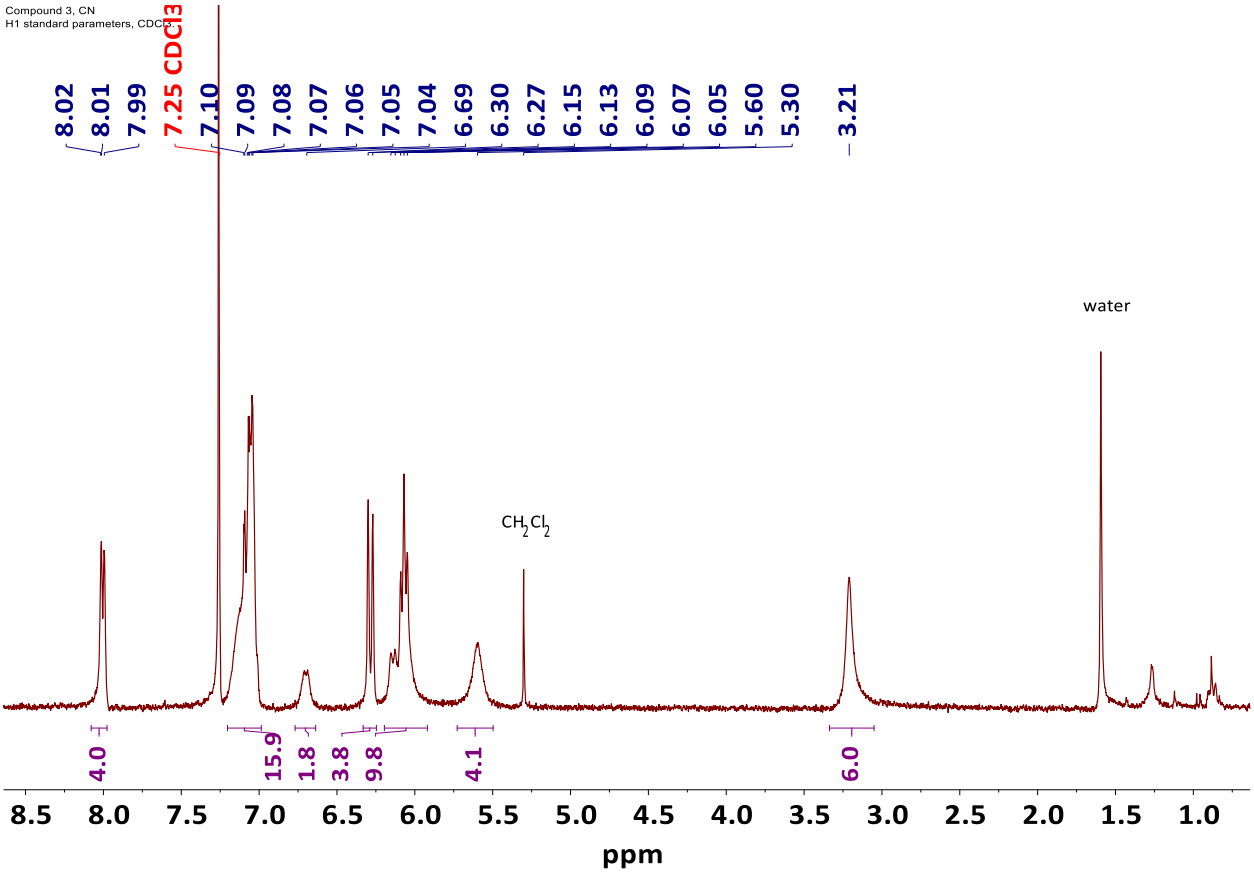

Figure S4. ^{1}H NMR spectrum of **2** in $CDCl_3$ at 293 K.

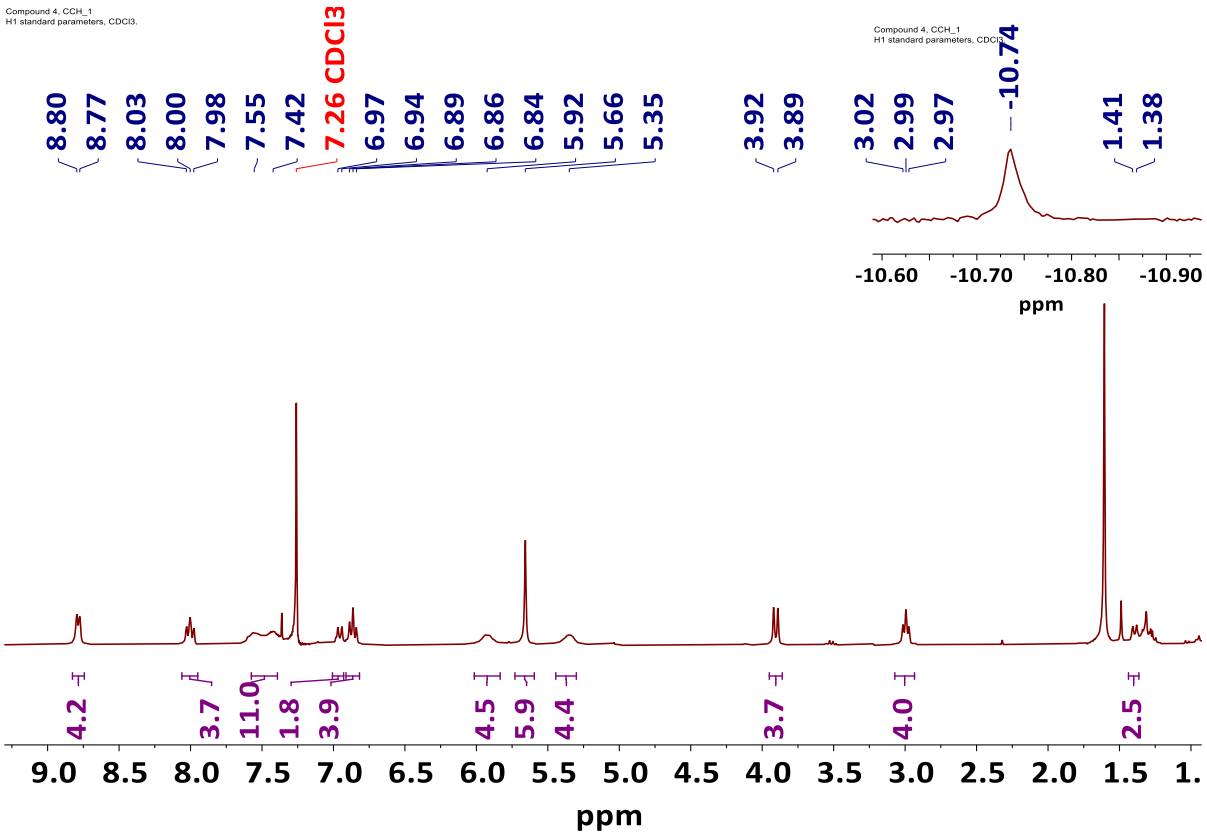

Figure S5. ^{1}H NMR spectrum of **3** in $CDCl_3$ at 293 K.

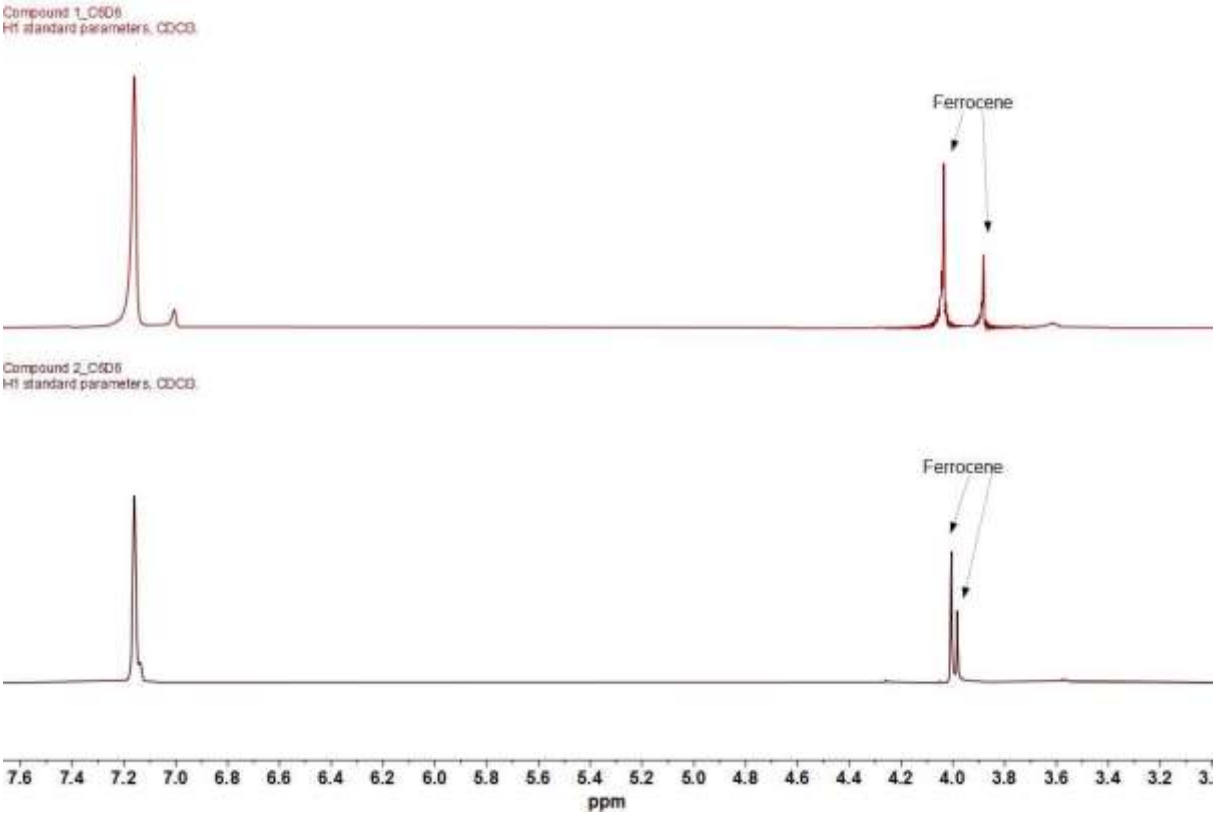

Figure S6. ^{1}H NMR spectra of **1** (top) and **4** (bottom) in C_6D_6 at 293 K, containing capillary inserts for Evans method[10] magnetometry.

$$\chi_m = \frac{3000 \times \Delta f \times 300}{F \times 4\pi \times [Ru_2]}$$

(where F = frequency of the spectrometer in Hz, Δf = difference in chemical shifts of Fc peak in ppm, $[Ru_2]$ = concentration of the diruthenium species in mol.L^{-1})

Using the above equation and applying appropriate diamagnetic corrections,[11] μ_{eff} for compound **1** and **4** were calculated:

$\mu_{eff,\mathbf{1}}$ = 4.1 μ_B; $\mu_{eff,\mathbf{4}}$ = 1.9 μ_B.

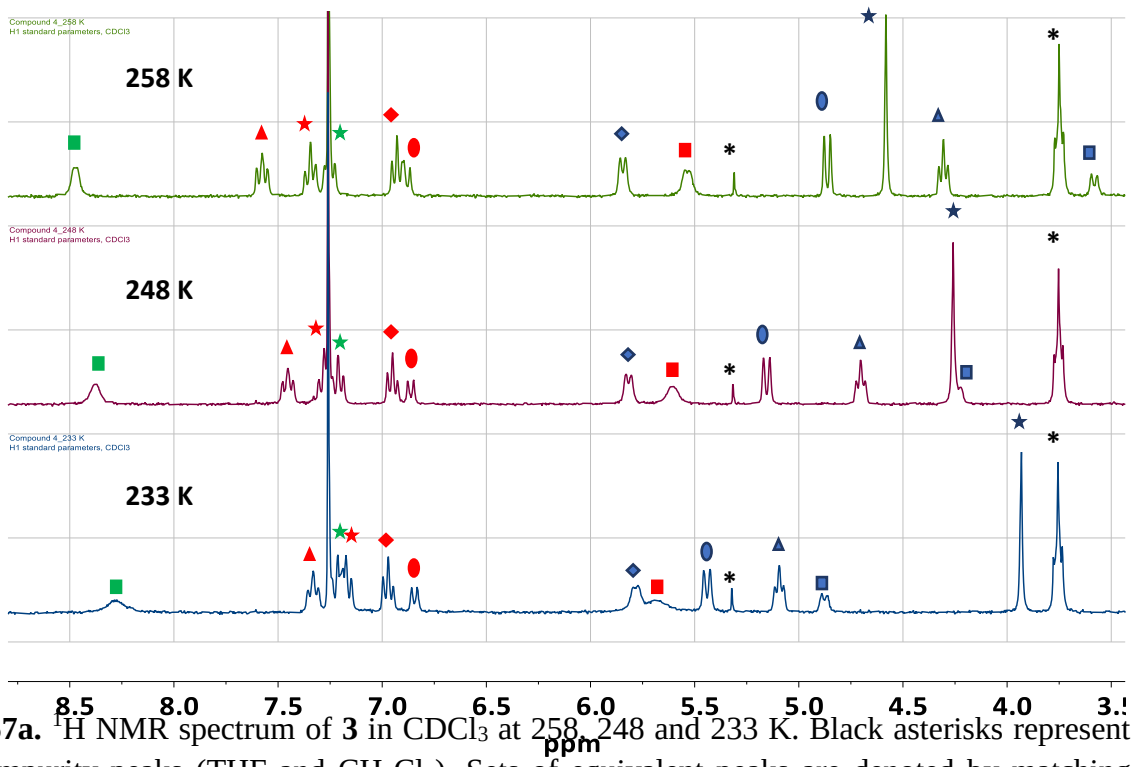

Figure S7a. ^{1}H NMR spectrum of **3** in $CDCl_3$ at 258, 248 and 233 K. Black asterisks represent solvent impurity peaks (THF and CH_2Cl_2). Sets of equivalent peaks are denoted by matching shapes and colors. See Figure S5 for the corresponding spectrum at 293 K.

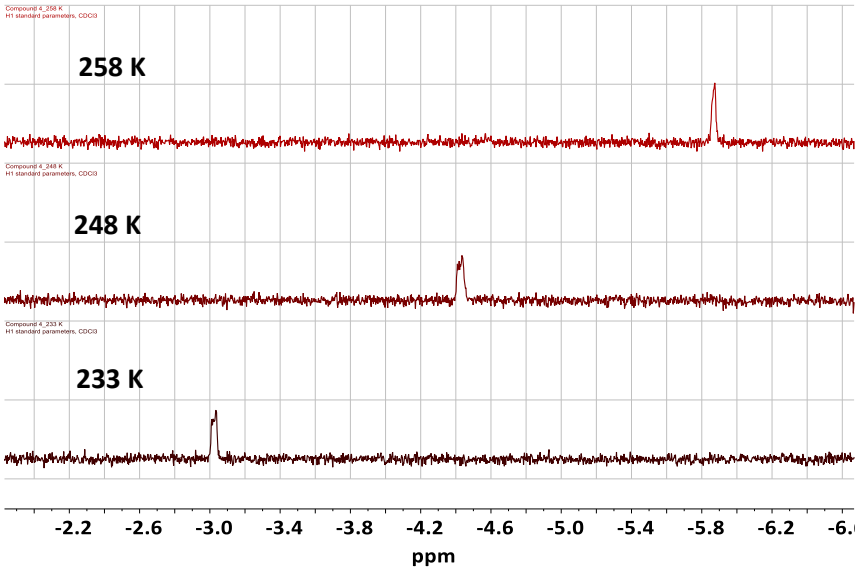

Figure S7b. ^{1}H NMR spectrum of **3** in $CDCl_3$ at 258, 248 and 233 K, shown here are the peaks corresponding to the acetylide (C≡C–**H**) proton.

It is clear from the above VT-NMR spectra that the chemical shifts for compound **3** are temperature-dependent. As the temperature is decreased, all the peaks trend toward their diamagnetic reference values. We thus hypothesize that compound **3** exists in a singlet ground state ($\lim_{T\to 0}(S) = 0$) but has a thermally accessible low-lying triplet state (S = 1). This can be modelled as the result of a Boltzmann distribution between the states according to equation EQ1.[12]

$$\delta(T) = a + \left(\frac{1}{T}\right)\frac{b.e^{\frac{c}{RT}}}{1+3e^{\frac{c}{RT}}} \ldots EQ1$$

a = δ_0, the diamagnetic reference value for the chemical shift of the proton considered,

b = a parameter that is related to the Hyperfine coupling constant,

c = $\Delta E_{s\text{-}t} = E_s - E_t$, the energy difference between the singlet ground state and the triplet excited state.

The parametrized equation (EQ1) was used to analyze the chemical shifts of the C≡C–**H**, N(C**H**$_3$)$_2$ and axial aryl(C**H**) protons (Figures S8a–c). Accordingly, the singlet-triplet energy gap was found to be $|2J| = 972.3 \pm 146.9$ cm^{-1} (2.78 ± 0.42 kcal/mol).

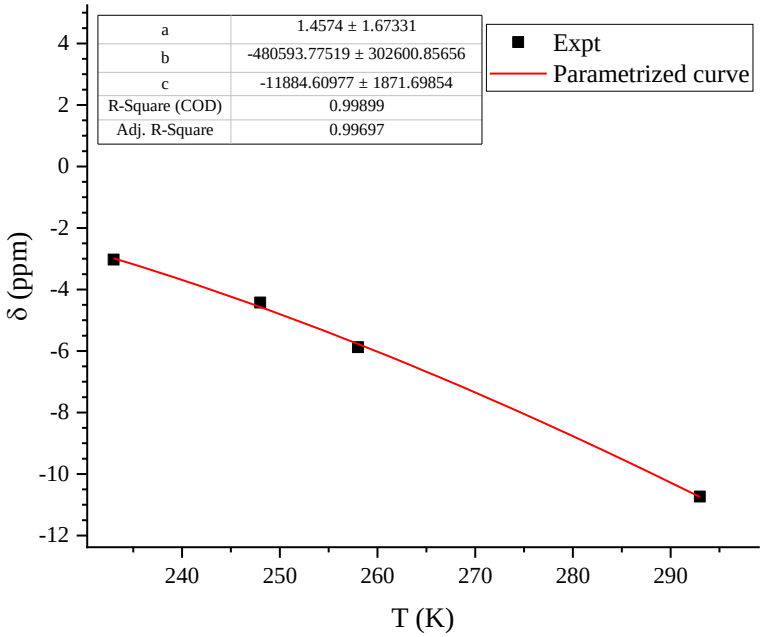

Figure S8a. Experimental VT-NMR chemical shift data for δ(C≡C–**H**) modelled according to the parametrized equation EQ1.

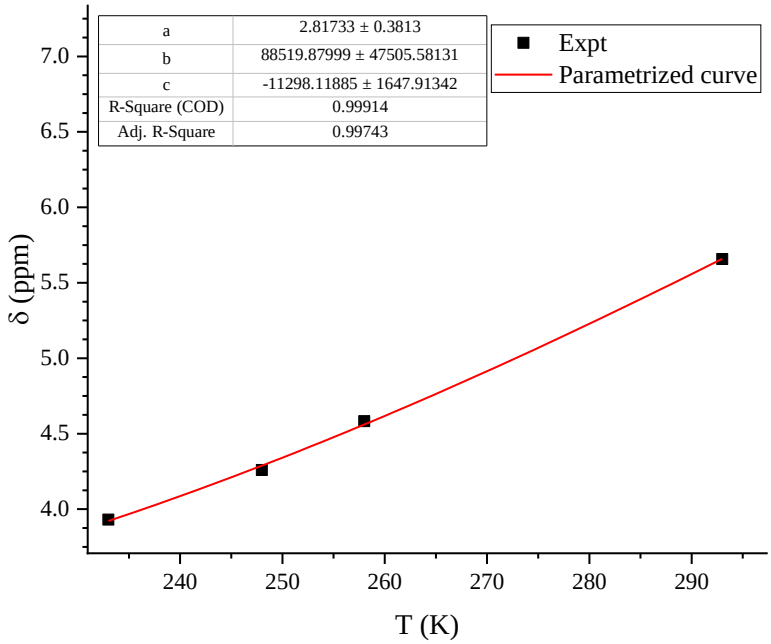

Figure S8b. Experimental VT-NMR chemical shift data for δ(N–(C**H**$_3$)$_2$) modelled according to the parametrized equation EQ1.

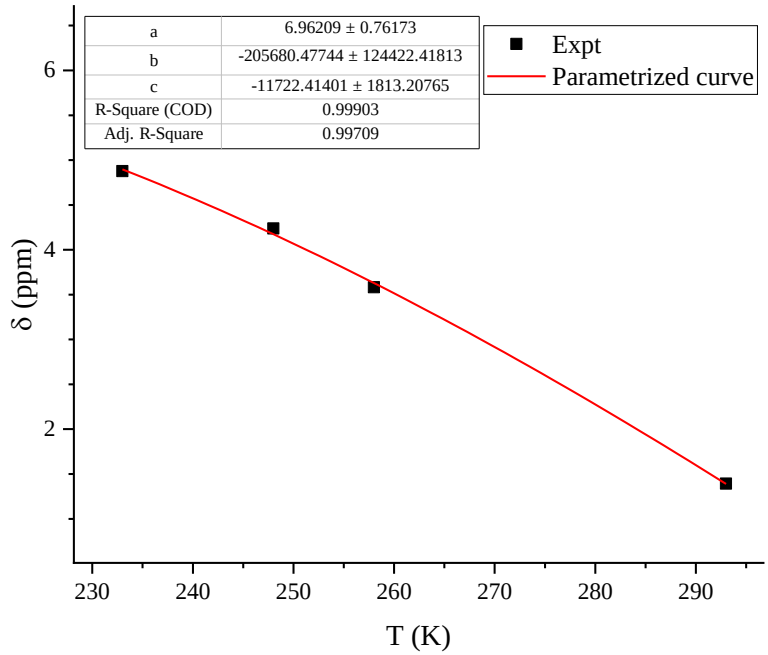

Figure S8c. Experimental VT-NMR chemical shift data for δ(Aryl(C**H**)) modelled according to the parametrized equation EQ1.

ELECTROCHEMISTRY

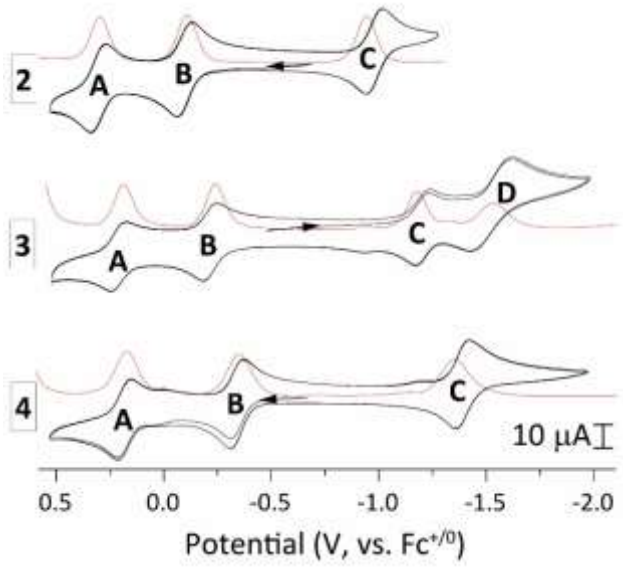

Figure S9. Cyclic (black) and differential pulse (red) voltammograms of compounds **2**–**4** recorded in 0.2 M $TBAPF_6$ THF. [Ru_2] is always ca. 1.0 mM.

Table S5. Redox potentials (V, versus $Fc^{+/0}$) for (Y)[Ru_2(*ap*)$_4$](C_6H_4-4-NMe_2)

Y	$E_{1/2}$ (**A**)	$E_{1/2}$ (**B**)	$E_{1/2}$ (**C**)	$E_{1/2}$ (**D**)
– (**1**)	0.12	−0.27 ($Ru_2^{6+/5+}$)	−1.62 ($Ru_2^{5+/4+}$)	-
CN (**2**)	0.30	−0.11 ($Ru_2^{7+/6+}$)	−0.98 ($Ru_2^{6+/5+}$)	-
C≡CH (**3**)	0.21	−0.21 ($Ru_2^{7+/6+}$)	−1.2 ($Ru_2^{6+/5+}$)	−1.53
CO (**4**)	0.18	−0.34 ($Ru_2^{6+/5+}$)	−1.39 ($Ru_2^{5+/4+}$)	-

Table S6. Voltammetry and IR spectroscopy of Ru_2–CO complexes in the literature

Compound	Oxidation state	$E_{1/2}$ (V *vs.* $Fc^{+/0}$)		ν_{CO}, cm^{-1}	Reference
		$Ru_2^{6+/5+}$	$Ru_2^{5+/4+}$		
$[Ru_2(dpb)_4(CO)]^+$	Ru_2^{5+}	0.48	−0.82	2013	[13]
$[Ru_2(DPhF)_4(CO)]^+$		-	-	2019	[14]
$[Ru_2(DPhF)_3(OAc)(CO)]^+$		0.31	−0.59	2016	[15]
[(CO)Ru_2(ap)$_4$Ar]		**−0.34**	**−1.39**	**1950**	**This work**
$Ru_2(dpb)_4(CO)$	Ru_2^{4+}	0.59	−0.37	1924	[13]
$Ru_2(DPhF)_4(CO)$		-	−0.20	1929	[14]
$[Ru_2(dpb)_4(CO)]^-$	Ru_2^{3+}	-	-	1834	[13]
$[Ru_2(DPhF)_4(CO)]^-$		-	-	1840	[14]

DISSOCIATION OF CO FROM (4)

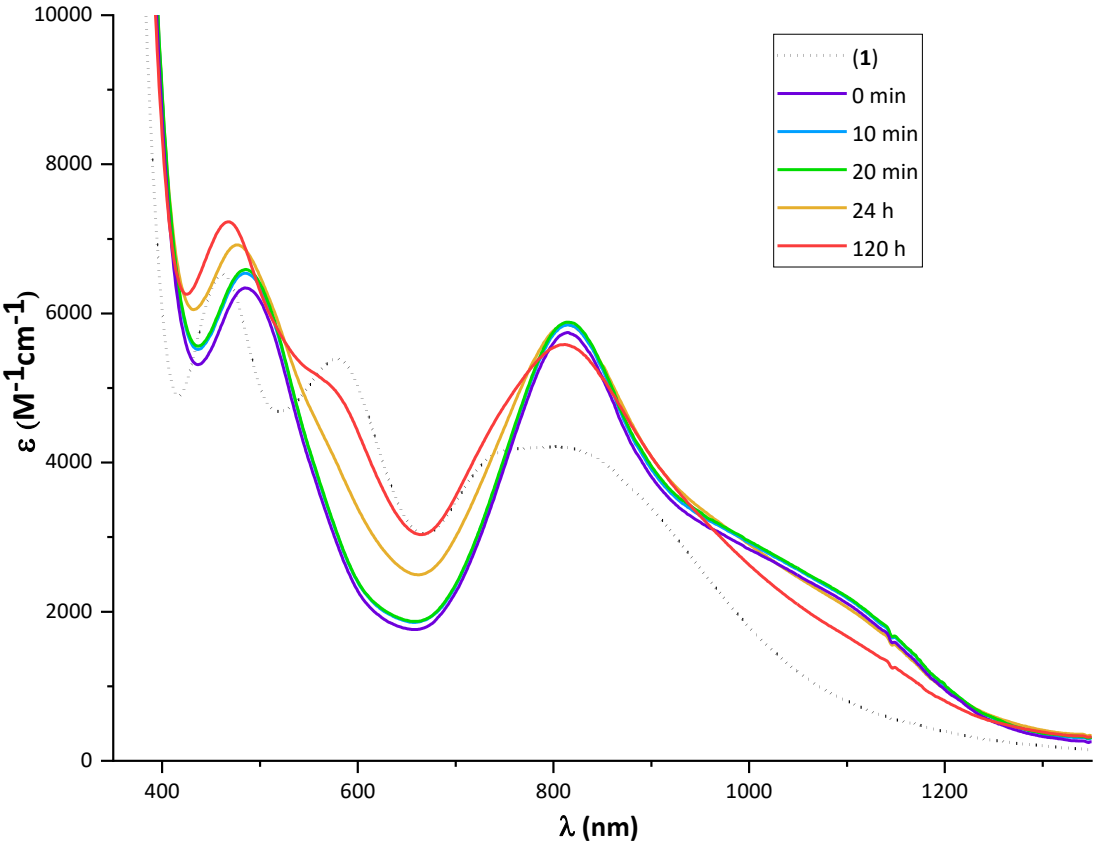

Figure S10. UV-Vis/NIR spectrum of **1** (black dotted line), **4** freshly prepared by exposure of **1** to CO, and slow dissociation of CO upon exposure to air for varying lengths of time.

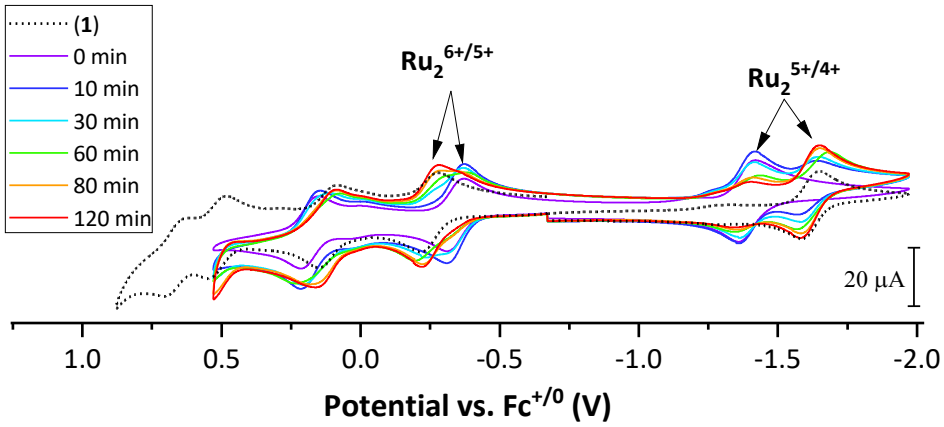

Figure S11. Cyclic voltammogram of compound **1** under N_2 (black dotted line), **4** freshly prepared by purging the electrochemical cell with CO (violet line, 0 min), and subsequent scans recorded after the electrochemical cell was purged with N_2 for varying lengths of time.

SQUID MAGNETOMETRY

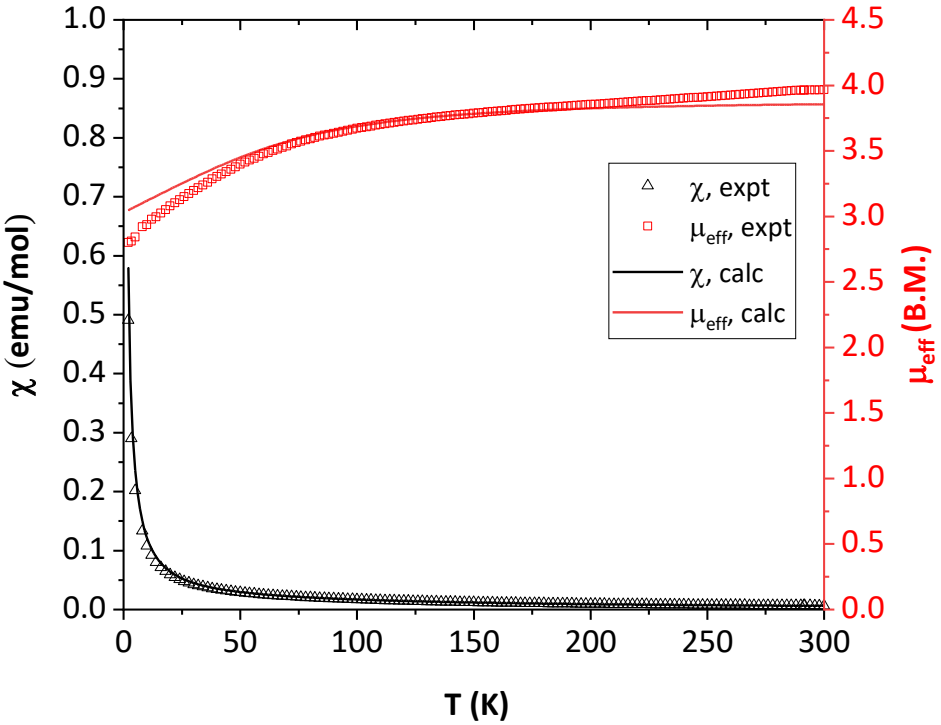

Figure S12. SQUID magnetometry data for **1** from 2 K – 300 K. Open symbols denote experimental values; solid lines denote simulated curves.

Compound **1**, which has a quartet ground state exhibits a temperature-dependent magnetic susceptibility varying over the range of 2 K – 300 K that can be fit according to the following equations:

$$\chi_{\parallel} = \frac{N_A g_{\parallel}^2 \beta^2}{k_B T} \cdot \left\{ \frac{1 + 9e^{-\frac{D}{k_B T}}}{4\left(1 + e^{-\frac{D}{k_B T}}\right)} \right\} \ldots EQ2$$

$$\chi_{\perp} = \frac{N_A g_{\perp}^2 \beta^2}{k_B T} \cdot \left\{ \frac{4 + \left(\frac{6k_B T}{D}\right)\left(1 - e^{-\frac{D}{k_B T}}\right)}{4\left(1 + e^{-\frac{D}{k_B T}}\right)} \right\} \ldots EQ3$$

$$\chi_{total} = \frac{1}{3}(\chi_{\parallel} + 2.\chi_{\perp}) \ldots EQ4$$

Where N_A = Avogadro's number, k_B = Boltzmann constant, T = temperature, D = Zero Field Splitting (ZFS) parameter, β = Bohr Magneton.

The curve in Figure S12 was simulated for D = 152 cm^{-1}, $g_{\parallel}$ = 1.9500, $g_{\perp}$ = 2.0265.

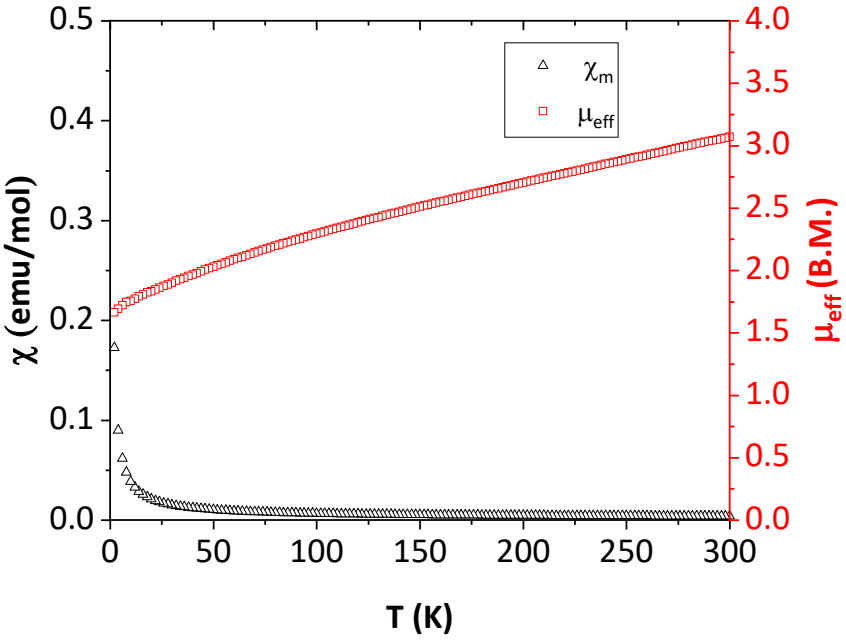

Figure S13. SQUID magnetometry data for **4** from 2 K – 300 K.

For a doublet ground state, the value of χT, and hence μ_{eff}, is expected to be invariant of temperature. However, the lability of CO and the associated change in spin-state complicates the issue. Ideally, the SQUID sample holder would be hermetically sealed under a magnetically inert atmosphere. But in the event of leaks wherein the compound gets inadvertently exposed to the low-pressure of the vacuum that is operative during measurements, CO can dissociate from the complex. All attempts to fit the data as a physical mixture of compound **4** (S = ½) with compound **1** (S = 3/2) as an impurity failed.

Upon closer inspection, it can be seen that with CO as a labile axial ligand, this system closely resembles $[Ru_2(DPhF)_3(OAc)(H_2O)]BF_4$,[16] which has labile water molecules at the axial positions. This compound displays a very similar magnetic behavior between 2 K – 300 K, which has been explained via a quantum mechanical spin admixture that takes place through spin-orbit coupling. This phenomenon could be operative in the case of compound **4** as well.

COMPUTATIONAL DETAILS

All Density Functional Theory (DFT) calculations were carried out using Gaussian16.[17] Geometry optimizations of **4** based on the corresponding crystal structure were done using the spin-unrestricted formalism with the B3LYP[18-21] and BP86[22] functionals. Minima were confirmed through frequency analysis. The output from B3LYP was found to be closer to experimentally determined metrical parameters. Table S6 lists the comparison between experimental and DFT-optimized structures (**4** and **4′**, respectively). Time-dependent DFT calculations (TD-DFT) were also performed on the optimized structure **4′** using both the B3LYP and BP86 functionals; BP86 gave large deviations from the experimental UV-Vis spectrum compared to B3LYP. All subsequent analyses, therefore, were performed with the B3LYP functional, basis sets def2-TZVP (with ECP) for Ru atoms and def2-SVP for C, H, O and N atoms,[23,24] and the polarizable continuum solvent model (CPCM) for tetrahydrofuran.

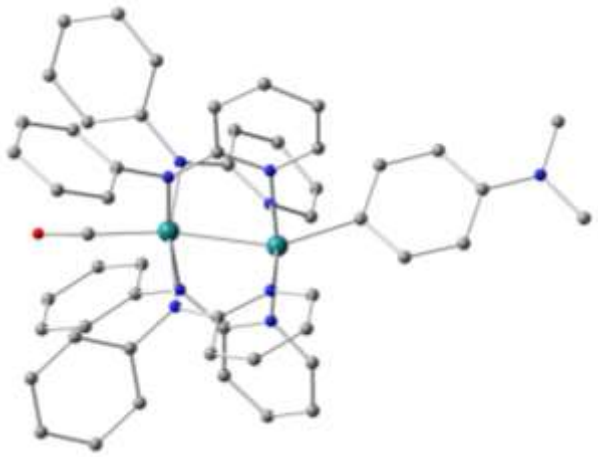

Figure S14. DFT-optimized structure (**4′**) derived from the single crystal X-ray diffraction data of compound **4**.

Table S7. Selected experimental and DFT-optimized metrical parameters of **4** and **4′**.

	4 (XRD)	**4′ (DFT, B3LYP)**	**4′ (DFT, BP86)**
Ru1−Ru2	2.5060(3)	2.52113	2.54806
Ru1−C1	2.053(2)	2.02168	2.03964
Ru2−C53	1.877(2)	1.85911	1.84910
C53−O1	1.146(2)	1.15457	1.17423
Ru2−Ru1−C1	155.61(6)	150.41711	151.40244
Ru1−Ru2−C53	169.50(7)	170.60788	169.55364

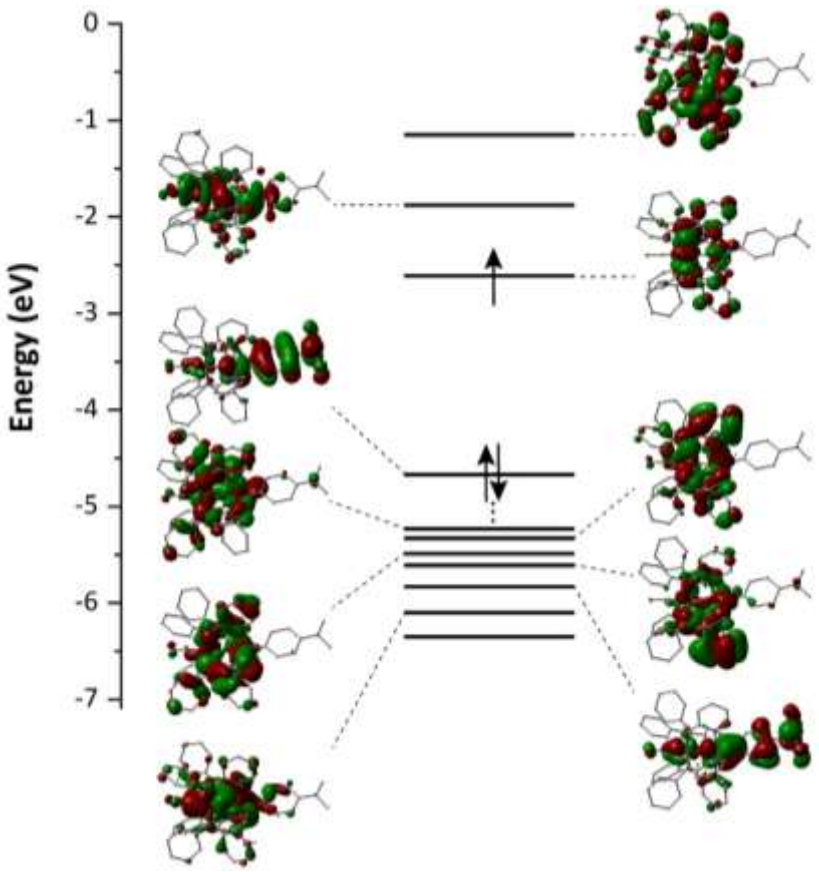

Figure S15. Frontier Molecular Orbitals of **4′** (energies in eV) represented at isovalue = |0.02|

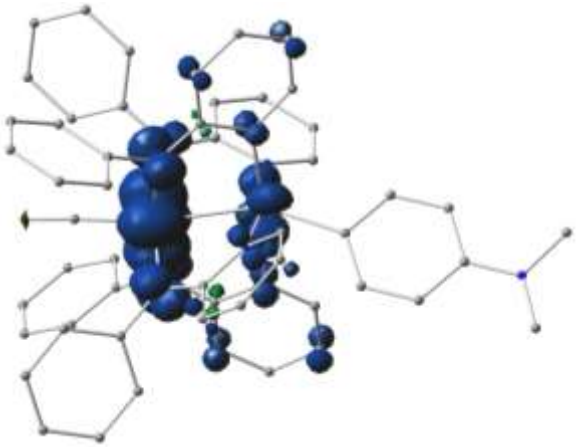

Figure S16. Net unpaired electron density calculated for **4′**, represented at |isovalue| = 0.003. The unpaired electron is predominantly localized on the δ* orbital, per the electronic configuration described in the text (also see Figure S15, SOMO)

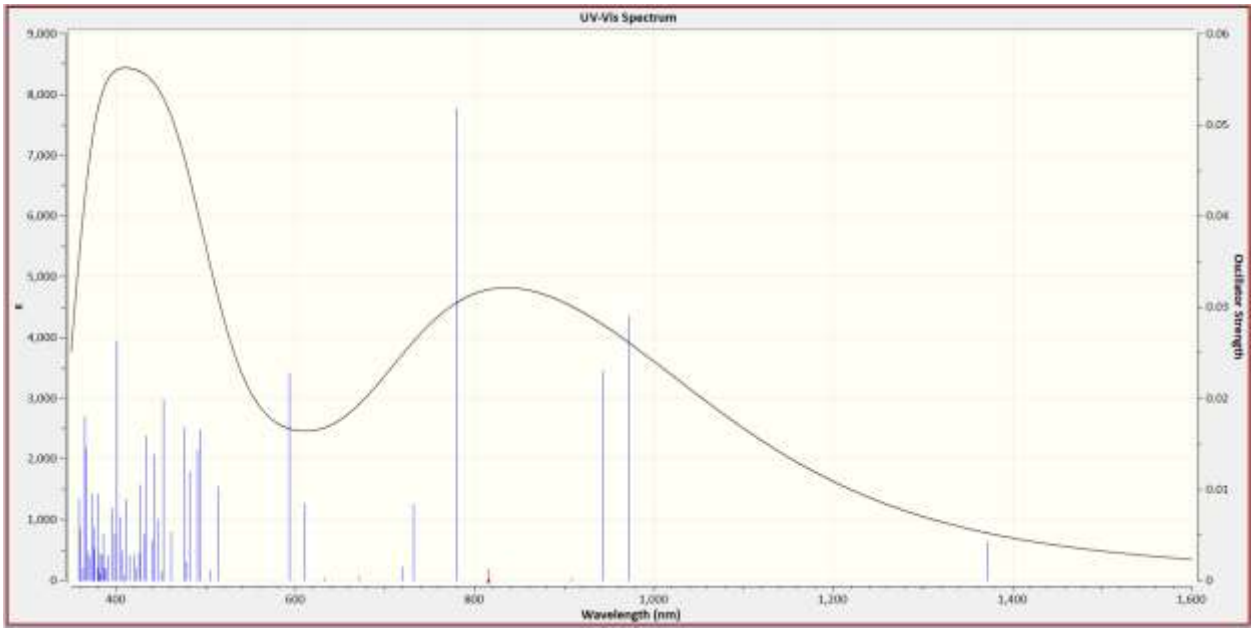

Figure S17. TD-DFT spectrum of DFT-optimized **4′** (compare with experimental spectrum in Figure S10)

REFERENCES:

(1) Zou, G.; Alvarez, J. C.; Ren, T. Ru-s-alkynyl compounds of tetraanilinopyridinato-diruthenium(II,III) core: Synthesis and structural characterization. *J. Organomet. Chem.* **2000**, *596*, 152-158.

(2) Raghavan, A.; Mash, B. L.; Ren, T. Forging Ru-C sp 2 Bonds in Paddlewheel Complexes Using the Lithium-Halogen Exchange Reaction. *Inorg. Chem.* **2019**, *58*, 2618-2626.

(3) Bear, J. L.; Chen, W. Z.; Han, B.; Huang, S.; Wang, L. L.; Thuriere, A.; Van Caemelbecke, E.; Kadish, K. M.; Ren, T. Cyanide adducts on the diruthenium core of $[Ru_2(L)_4]^+$ (L = ap, CH_3ap, Fap, or F_3ap). Electronic properties and binding modes of the bridging ligand. *Inorg. Chem.* **2003**, *42*, 6230-6240.

(4) Chakravarty, A. R.; Cotton, F. A.; Tocher, D. A. Syntheses, molecular structures, and properties of two polar diruthenium(II,III) complexes of 2-hydroxypyridine and 2-anilinopyridine. *Inorg. Chem.* **1985**, *24*, 172-177.

(5) Xu, G.; Ren, T. Ru-s-butadiynyl complexes of the tetraanilinopyridinatodiruthenium core: Formation of a bis-adduct. *Organometallics* **2001**, *20*, 2400-2404.

(6) Chen, W. Z.; Silva, V. D.; Lin, C.; Abellard, J.; Marcus, D. M.; Ren, T. Azidotetrakis(diarylformamidinate)diruthenium(II,III) Compounds: Synthesis, Molecular Structures and Voltammetric Properties; Linear Free Energy Relationships in Dinuclear Compounds VII. *J. Cluster Sci.* **2005**, *16*, 151-165.

(7) Sheldrick, G. M. In *Acta Cryst*, 2008; Vol. A64; pp 112-112.

(8) Sheldrick, G. M. Crystal structure refinement with SHELXL. *Acta Cryst. C* **2015**, *71*, 3-8.

(9) Sheldrick, G. M. SHELXL 2016; University of Göttingen, Germany. **2016**.

(10) Evans, D. F. The Determination of the Pararnagnetic Susceptibility. *J. Chem. Soc.* **1959**, 2003-2005.

(11) Bain, G. A.; Berry, J. F. Diamagnetic corrections and Pascal's constants. *J. Chem. Educ.* **2008**, *85*, 532-536.

(12) Guennic, B. L.; Floyd, T.; Galan, B. R.; Autschbach, J.; Keister, J. B. Paramagnetic effects on the NMR spectra of "diamagnetic" ruthenium (bis-phosphine)(bis-semiquinone) complexes. *Inorg. Chem.* **2009**, *48*, 5504-5511.
(13) Manowong, M.; Han, B.; McAloon, T. R.; Shao, J.; Guzei, I. A.; Ngubane, S.; Van Caemelbecke, E.; Bear, J. L.; Kadish, K. M. Effect of axial ligands on the spectroscopic and electrochemical properties of diruthenium compounds. *Inorg. Chem.* **2014**, *53*, 7416-7428.
(14) Kadish, K. M.; Han, B.; Shao, J.; Ou, Z.; Bear, J. L. Synthesis and characterization of diruthenium complexes in low oxidation states. Formation of mono- and bis-CO adducts. *Inorg. Chem.* **2001**, *40*, 6848-6851.
(15) Barral, M. C.; Herrero, S.; Jimenez-Aparicio, R.; Torres, M. R.; Urbanos, F. A. Carbonyl and nitrosyl diruthenium compounds: Crystal structure of [Ru2(O2CMe)(DPhF)3(CO)]BF4 Â· CH2Cl2 and its isomorphous nitrosyl analogue. *J. Organomet. Chem.* **2008**, *693*, 1597-1604.
(16) Barral, M. C.; Herrero, S.; Jimenez-Aparicio, R.; Torres, M. R.; Urbanos, F. A. A spin-admixed ruthenium complex. *Angew. Chem. Int. Ed.* **2005**, *44*, 305-307.
(17) *Gaussian 16 Rev. A.03*; Frisch, M. J.; Trucks, G. W.; Schlegel, H. B.; Scuseria, G. E.; Robb, M. A.; Cheeseman, J. R.; Scalmani, G.; Barone, V.; Petersson, G. A.; Nakatsuji, H.; Li, X.; Caricato, M.; Marenich, A. V.; Bloino, J.; Janesko, B. G.; Gomperts, R.; Mennucci, B.; Hratchian, H. P.; Ortiz, J. V.; Izmaylov, A. F.; Sonnenberg, J. L.; Williams; Ding, F.; Lipparini, F.; Egidi, F.; Goings, J.; Peng, B.; Petrone, A.; Henderson, T.; Ranasinghe, D.; Zakrzewski, V. G.; Gao, J.; Rega, N.; Zheng, G.; Liang, W.; Hada, M.; Ehara, M.; Toyota, K.; Fukuda, R.; Hasegawa, J.; Ishida, M.; Nakajima, T.; Honda, Y.; Kitao, O.; Nakai, H.; Vreven, T.; Throssell, K.; Montgomery Jr., J. A.; Peralta, J. E.; Ogliaro, F.; Bearpark, M. J.; Heyd, J. J.; Brothers, E. N.; Kudin, K. N.; Staroverov, V. N.; Keith, T. A.; Kobayashi, R.; Normand, J.; Raghavachari, K.; Rendell, A. P.; Burant, J. C.; Iyengar, S. S.; Tomasi, J.; Cossi, M.; Millam, J. M.; Klene, M.; Adamo, C.; Cammi, R.; Ochterski, J. W.; Martin, R. L.; Morokuma, K.; Farkas, O.; Foresman, J. B.; Fox, D. J.: Wallingford, CT, 2016.
(18) Vosko, S. H.; Wilk, L.; Nusair, M. Accurate spin-dependent electron liquid correlation energies for local spin density calculations: a critical analysis. *Can. J. Phys.* **1980**, *58*, 1200-1211.
(19) Becke, A. D. Density-functional exchange-energy approximation with correct asymptotic behavior. *Phys. Rev. A* **1988**, *38*, 3098-3100.
(20) Becke, A. D. Density-functional thermochemistry. III. The role of exact exchange. *J. Chem. Phys.* **1993**, *98*, 5648-5652.
(21) Stephens, P. J.; Devlin, F. J.; Chabalowski, C. F.; Frisch, M. J. Ab Initio Calculation of Vibrational Absorption and Circular Dichroism Spectra Using Density Functional Force Fields. *J. Phys. Chem.* **1994**, *98*, 11623-11627.
(22) Perdew, J. P. Density-functional approximation for the correlation energy of the inhomogeneous electron gas. *Phys. Rev. B* **1986**, *33*, 8822-24.
(23) Andrae, D.; Häußermann, U.; Dolg, M.; Stoll, H.; Preuß, H. Energy-adjusted ab initio pseudopotentials for the second and third row transition elements. *Theor. Chim. Acta* **1990**, *77*, 123-141.
(24) Weigend, F.; Ahlrichs, R. Balanced basis sets of split valence, triple zeta valence and quadruple zeta valence quality for H to Rn: Design and assessment of accuracy. *Phys. Chem. Chem. Phys.* **2005**, *7*, 3297-3305.